Microplane model for stiff foams and finite element analysis of sandwich failure by core indentation

Michele Brocca [a], Zdeněk P. Bažant [b,*], Isaac M. Daniel [c]

[a] *Department of Civil Engineering, Northwestern University, Evanston, IL 60208, USA*
[b] *Walter P. Murphy Professor of Civil Engineering and Materials Science, Northwestern University, Evanston, IL 60208, USA*
[c] *Walter P. Murphy Professor of Civil and Mechanical Engineering, Northwestern University, Evanston, IL 60208, USA*

Abstract

Composite sandwich plates and shells are gaining increasing popularity in engineering practice, due to their high stiffness-to-weight ratio, low thermal conductivity and energy absorption characteristics. Modeling of the structural response of a sandwich member requires knowledge of the mechanical behavior of the materials used for the facings and the core. The paper presents a new constitutive model for closed-cell cellular materials, developed with the microplane approach. The model is then employed in a finite element analysis of three point bending tests of sandwich beams failing by core indentation. Good agreement of the numerical results with the experimental observations is achieved. This proves the new model to be capable of satisfactorily reproducing the mechanical response of cellular materials. © 2001 Elsevier Science Ltd. All rights reserved.

Keywords: Composites; Sandwich plates; Foams; Cellular materials; Finite-element analysis

1. Introduction

Sandwich plates and shells are structural members consisting of two stiff and strong faces (skins) separated by a light-weight core. By increasing the cross-sectional moment of inertia of the pair of faces, the presence of the core increases the flexural stiffness of sandwich members without significant increase in weight. Sandwich structures are found in nature and are commonly used in engineering design whenever it is necessary to minimize the weight of the structure (typically in the automobile and aerospace industries, and also in civil engineering). Aside from low weight, sandwich panels are also characterized by low thermal conductivity, high energy absorption and good damping properties.

The materials used for the core and the faces vary. Most commonly used for the core are honeycombs or cellular materials (rigid foams), produced from metals, polymers or ceramics. The faces (or facings) are usually made of metals or composites.

* Corresponding author. Address: Department of Civil Engineering, The Technological Institute, 2145 Sheridan Road, Evanston, IL 60208-3109, USA. Fax: +1-847-491-3109.

E-mail address: z-bazant@northwestern.edu (Z.P. Bažant).

Sandwiches can fail in several different ways (for a detailed discussion see, e.g., Triantafillou and Gibson (1987)). Faces may fail by yielding, crushing or elastic buckling, and the core can fracture or yield. In general, the overall failure of the member includes a combination of these failure modes occurring in both the core and the faces, the combination being determined by the particular configuration of the structure, by the loading conditions and by the boundary conditions.

Modeling of sandwiches requires knowledge of the mechanical behavior of the materials used for the facings and the core. This paper presents a model for rigid, low-density, closed-cell cellular materials, developed with the microplane model approach, which will be employed in finite element analysis of failure of sandwich beams by core indentation.

Attention will be focused on failure by core indentation, because this kind of failure of the foam in the core is dominated by finite strain, and provides the most severe check for the newly introduced material model.

The objective of this paper is twofold: to develop a numerical tool for structural analysis of sandwich beams and, at the same time, to give an example of how the microplane model can be effectively used to formulate the constitutive law of a complex materials such as foam in terms of vectors rather than tensors. At this stage we consider only a simple model, whose performance is comparable to that of the already existing tensorial models (e.g., Puso and Govindjee, 1995). However the microplane approach is appealing in that it provides a robust and powerful basis for further refinements and generalizations.

The structure of the paper will be as follows: Section 2 will briefly describe the mechanical behavior of foams. Section 3 will review the basic formulation of the microplane model for the small-strain range. In Section 4, a microplane model for closed-cell stiff foams will be introduced and a discussion will be given on how to extend in this case the microplane model to the finite strain range. A few possible refinements and modifications of the model will also be considered. Section 5 will provide information about the experiments whose results are analyzed in order to validate the model. Finally, Sections 6–8 will present the formulation and the results of finite element analysis of sandwich beams based on the new model for foam.

2. Mechanical behavior of foams

Among the existing cellular materials, only polymeric foams are considered in this study. Foamed plastics, also referred to as cellular or expanded plastics, are good heat insulators by virtue of the low conductivity of the gas contained in the cells. They have a higher ratio of flexural modulus to density than before foaming. They achieve a greater load-bearing capacity per unit weight, as well as greater energy storage and energy dissipation capacities. Examples of commonly produced foamed plastics are polyurethane, PVC, polystyrene, polypropylene, epoxy, phenol–formaldehyde, ABS, cellulose acetate, silicone, etc. It is virtually possible to produce every thermoplastic and thermoset polymer in a cellular form.

Foamed plastics can be classified according to the nature of the cells into closed-cell and open-cell types. In a closed-cell type of foam, each individual cell, more or less spherical in shape, is completely enclosed by a wall of plastic, while in an open-cell type of foam the individual cells are interconnected, as in a sponge. Free expansion during cell formation usually produces open-cell foams. Closed-cell foams are produced in processes where some pressure is maintained during the cell formation stage. Foamed plastics are produced in a wide range of densities: from 0.001 to 0.96 g/cm^3. They are also classified into flexible, semi-rigid, rigid. A foam is said to be rigid if the polymer matrix exists in the crystalline state or, if amorphous, is below its glass transition temperature, T_g. A foam is said to be flexible if the matrix polymer is above its T_g.

The shape, size and distribution of cells can be very regular or highly inhomogeneous, depending on the particular material and foaming process adopted. Accordingly, polymer foams may be homogeneous, with a uniform cellular morphology throughout, or they may be structurally anisotropic. Viscous forces during cell formation usually produce cells elongated in one direction (rise direction), thus giving constitutive
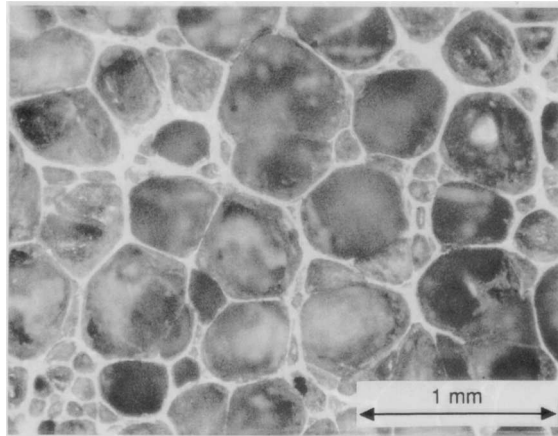
Fig. 1. Morphology of closed-cell foam H130 from Divinycell. Relative density, $\rho/\rho_M = 130/1400 = 0.093$ (after Grenested, 1999).

properties with an approximate cylindrical symmetry. This happens when the foaming process is done in a mold and the volume expansion makes the foam rise in one direction (Gibson and Ashby, 1997; Huber and Gibson, 1988). Fig. 1 (after Grenestedt, 1999) shows a microphotograph of a PVC foam similar to that used in the sandwich beam tests analyzed in this paper. As seen from the figure, the cell sizes for this particular foam are very inhomogeneous locally, but have an overall uniform morphology.

Foaming of plastics can be achieved in several ways. One possibility is to create gases inside the mass of the polymer. Once the polymer has been expanded, the cellular structure must be stabilized rapidly. If the polymer is thermoplastic, the expansion is carried out above the melting point, and the foam is then immediately cooled below the melting point (such a process is referred to as physical stabilization). Otherwise chemical stabilization can be performed. Air can be whipped into a solution of the plastic, low boiling liquid, or incorporated in the plastic mix and then volatilized by heat. Carbon dioxide gas can be produced within the plastic mass by chemical reaction, or other gases (e.g., nitrogen) can be dissolved in the plastic melt under pressure and then allowed to expand by reducing the pressure as the melt is extruded. Gas can also be generated within the plastic mass by thermal decomposition of a chemical blowing agent.

An excellent discussion of typical uniaxial behavior of cellular materials can be found, e.g., in Gibson (1989), or Gibson and Ashby (1997). Gibson (1989) shows typical stress strain diagrams for cellular materials in tension and compression. In compression, after an initial elastic response and 'yield' plateau, the material suddenly stiffens due to densification of the material after pore collapse. In uniaxial tension, the cell walls align themselves in the direction of tension, which engenders recovery of stiffness after a certain amount of nonlinear deformation. The tensile and compressive stress–strain diagrams are typically asymmetric.

True yielding of the foam can be caused by irrecoverable plastic yield of the polymer; by apparent yielding in monotonic compression by recoverable elastic buckling of cell walls or by irrecoverable progressive brittle crushing of the cell walls. In the 'rigid' foams, the nonlinear deformation is usually irrecoverable. An important characteristic aspect is a zero value of 'plastic' Poisson's ratio: when a foam is yielding in uniaxial compression, very little transverse deformation is observed. This endows the foam with a shock adsorption capability (see Section 4 for more comments on this).

Several phenomenological models for cellular material have been proposed in the past, e.g., by Neilsen et al. (1987), Puso and Govindjee (1995), and Chang et al. (1998). The model proposed in this paper is based on the microplane model approach. As it will be shown in the following sections, this approach allows taking more directly into account the micromechanical source of the macroscopic mechanical behavior of

materials. This is a particularly advantageous feature for a material model, especially when dealing with highly nonlinear and complex materials.

3. The microplane model

3.1. History of microplane model

The essential idea of the microplane modeling approach is to characterize the constitutive law in terms of *vectors* rather than *tensors*. This idea can be traced back to a pioneering concept of Taylor (1938), who proposed characterizing the plastic hardening of polycrystalline metals by relations between the stress and strain vectors acting on planes of various possible orientations within the material and determining the macroscopic strain and stress tensors as a summation of all these vectors under the assumption of a static or kinematic constraint. Batdorf and Budiansky (1949) were the first to extend Taylor's concept with a static constraint and develop a realistic model for plasticity of polycrystalline metals, still considered among the best. Many other researchers subsequently refined or modified this approach to metals (Kröner, 1961; Budiansky and Wu, 1962; Lin and Ito, 1965; Hill, 1965, 1966; Rice, 1971). Extensions for the hardening inelastic response of soils and rocks have also been made (Zienkiewicz and Pande, 1977; Pande and Sharma, 1983).

All the aforementioned models used the so called 'static constraint': The assumption that the stress vector acting on a given plane in the material, called the microplane, is the projection of the macroscopic stress tensor. Bažant (1984) and Bažant and Oh (1985), found that, for stability reasons, a static constraint prevents the model from being generalized for postpeak behavior or softening damage typical of quasi-brittle materials. The extension to softening damage requires replacing the static constraint by a kinematic constraint, in which the strain vector on any inclined plane in the material is the projection of the macroscopic strain tensor.

In all applications to metals, the formulations emanating from Batdorf and Budiansky's work were called the slip theory of plasticity. This term, however, is unsuitable for general material models, for example models of the cracking damage in quasi-brittle materials, where the inelastic behavior on the microscale does not physically represent plastic slip. For this reason the neutral term 'microplane model', applicable to any type of inelastic behavior (Bažant, 1984), was coined. Microplane is the name given to a plane of any orientation in the material, used to characterize the microstructural behavior of the material.

After generalizing the microplane model for both tensile and compressive damage (Bažant and Prat, 1988a,b), the microplane model and the corresponding numerical algorithm reached its present, very effective formulation for concrete in Bažant et al. (2000a,b,c). Microplane formulations have also been developed for anisotropic clays (Bažant and Prat, 1987), for soils (Prat and Bažant, 1989, 1991a,b), for metals (Brocca and Bažant, 2000) and for shape-memory alloys (Brocca et al., 2000). A detailed review of the microplane model formulation with a kinematic or static constraint can be found in Carol and Bažant (1997). For both the formulations with kinematic and static constraints, the material properties are characterized by relations between the stress and strain components on the microplanes. The tensorial invariance restrictions need not be directly enforced in the constitutive relations, which is an advantageous feature of the microplane formulation. They are automatically satisfied by superimposing in a suitable manner the responses from the microplanes of all orientations. This is done by means of a variational principle (principle of virtual work) (Bažant, 1984). The fact that the constitutive law is described in terms of vectors rather than tensors endows the model with conceptual clarity and allows more realistic modeling of oriented phenomena such as friction or cracking. In the next paragraphs we will present the basic formulation for the microplane model for the case of small strains. The generalization to the finite strain range will be discussed in Section 4.

3.2. Formulation with kinematic constraint

The orientation of a microplane is characterized by the unit normal **n** of components n_i (indices i and j refer to the components in Cartesian coordinates x_i). In the formulation with kinematic constraint, which makes it possible to describe softening in a stable manner, the strain vector $\vec{\varepsilon}_N$ on the microplane (Fig. 2) is the projection of the macroscopic strain tensor ε_{ij}. So the components of this vector are $\varepsilon_{Ni} = \varepsilon_{ij} n_j$. The normal strain on the microplane is $\varepsilon_N = n_i \varepsilon_{Ni}$, that is

$$\varepsilon_N = N_{ij} \varepsilon_{ij}, \quad N_{ij} = n_i n_j, \tag{1}$$

where repeated indices imply summation over $i = 1, 2, 3$. The mean normal strain, called the volumetric strain ε_V, and the deviatoric strain ε_D on the microplane can also be introduced; they are defined as follows (for small strains):

$$\varepsilon_V = \varepsilon_{kk}, \qquad \varepsilon_D = \varepsilon_N - \tfrac{1}{3}\varepsilon_V = \tfrac{2}{3}(\varepsilon_N - \varepsilon_S), \tag{2}$$

where ε_S = spreading strain = mean normal strain in microplane. ε_S characterizes the lateral confinement of the microplane and the creation of splitting cracks normal to the microplane. Considering ε_V and ε_D (or ε_S) is useful when the effect of lateral confinement on compression failure needs to be described and when the volumetric–deviatoric interaction, observed for a number of cohesive frictional materials such as concrete, needs to be captured.

To characterize the shear strains on the microplane (Fig. 2), one needs to define two coordinate directions M and L, given by two orthogonal unit coordinate vectors **m** and **l** of components m_i and l_i lying on the microplane. To minimize directional bias of **m** and **l** among microplanes, one alternates among choosing vectors **m** to be normal to axis x_1, x_2 or x_3.

The magnitudes of the shear strain components on the microplane in the direction of **m** and **l** are $\varepsilon_M = m_i(\varepsilon_{ij} n_j)$ and $\varepsilon_L = l_i(\varepsilon_{ij} n_j)$. Because of the symmetry of tensor ε_{ij}, the shear strain components may be written as:

$$\varepsilon_M = M_{ij} \varepsilon_{ij}, \qquad \varepsilon_L = L_{ij} \varepsilon_{ij} \tag{3}$$
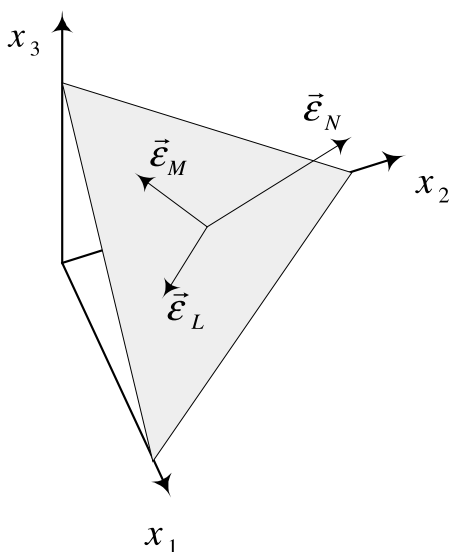

Fig. 2. Strain components on a microplane.

in which the following symmetric tensors are introduced:

$$M_{ij} = (m_i n_j + m_j n_i)/2, \qquad L_{ij} = (l_i n_j + l_j n_i)/2. \tag{4}$$

Once the strain components on each microplane are obtained, the stress components are updated through microplane constitutive laws, which can be expressed in an algebraic or differential form.

If the kinematic constraint is imposed, the stress components on the microplanes are equal to the projections of the macroscopic stress tensor σ_{ij} only in some particular cases, in which the microplane constitutive laws are specifically prescribed so that this condition be satisfied. This happens, for example, in the case of elastic laws at the microplane level, defined with elastic constants chosen so that the overall macroscopic behavior is the usual elastic behavior (see Carol and Bažant, 1997). In general, the stress components determined independently on the various planes will not be related to one another in such a manner that they could be considered as projections of a macroscopic stress tensor. Thus static equivalence or equilibrium between the microlevel stress components and macrolevel stress tensor must be enforced by other means. This can be accomplished by applying the principle of virtual work,

$$\sigma_{ij} = \frac{3}{2\pi} \int_\Omega \sigma_N n_i n_j \, d\Omega + \frac{3}{2\pi} \int_\Omega \frac{\sigma_{Tr}}{2} (n_i \delta_{rj} + n_j \delta_{ri}) \, d\Omega, \tag{5}$$

where Ω is the surface of a unit hemisphere. Eq. (5) is based on the equality of the virtual work inside a unit sphere and on its surface, rigorously justified by Bažant et al. (1996).

The integration in Eq. (5), is performed numerically by an optimal Gaussian integration formula for a spherical surface using a finite number of integration points on the surface of the hemisphere. Such an integration technique corresponds to considering a finite number of microplanes, one for each integration point. A formula consisting of 28 integration points is given by Stroud (1971). Bažant and Oh (1986) developed a more efficient and about equally accurate formula with 21 integration points, and studied the accuracy of various formulas in different situations.

3.3. Formulation with static constraint

A formulation with static constraint equates the stress components on each microplane to the projections of the macroscopic stress tensor σ_{ij}. Once the strain components on each microplane are updated by the use of the microplane constitutive laws, the macroscopic strain tensor is obtained again by applying the principle of virtual work.

The microplane components of stress are defined as follows:

$$\sigma_N = N_{ij}\sigma_{ij}, \quad N_{ij} = n_i n_j, \tag{6}$$

$$\sigma_M = M_{ij}\sigma_{ij}, \qquad \sigma_L = L_{ij}\sigma_{ij}, \tag{7}$$

where

$$M_{ij} = (m_i n_j + m_j n_i)/2, \quad L_{ij} = (l_i n_j + l_j n_i)/2. \tag{8}$$

The complementary virtual work equation provides, in analogy to Eq. (5),

$$\varepsilon_{ij} = \frac{3}{2\pi} \int_\Omega \varepsilon_N n_i n_j \, d\Omega + \frac{3}{2\pi} \int_\Omega \frac{\varepsilon_{Tr}}{2} (n_i \delta_{rj} + n_j \delta_{ri}) \, d\Omega. \tag{9}$$

Again, volumetric and deviatoric quantities can be introduced:

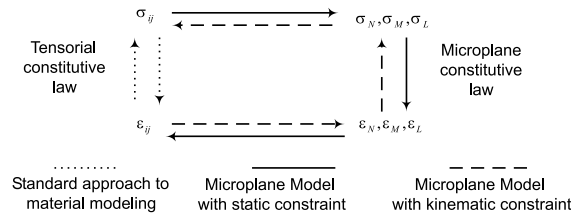$$\sigma_V = \sigma_{kk}/3, \qquad \sigma_D = \sigma_N - \sigma_V, \tag{10}$$

Fig. 3. Patterns for stress or strain update in the microplane model with static or kinematic constraint.

σ_V and σ_D are used when the effect of hydrostatic pressure and spreading stress or confining stress need to be accounted for explicitly.

3.4. Formulation with double constraint

It is possible and advantageous to formulate the microplane model with particular material laws such that a kinematic constraint for the strains coexists with a static constraint for the true stresses in the sense of damage mechanics (but of course not for the actual stresses). When this happens, the model is said to have a *double constraint* since it satisfies simultaneously the integral equations (5) for true stresses and Eq. (9) for strains. Such a double constraint is useful in microplane damage formulations (Carol and Bažant, 1997; Bažant et al., 1996, 2000b).

Fig. 3 shows schematically the pattern followed in order to update the stress or strain in the microplane model approach. As shown, the microplane model takes simple constitutive laws on each microplane and transforms them into a consistent three-dimensional model. In this work, the static constraint is used. Thus the macroscale stress tensor is projected onto the 28 or 21 microplanes using Eqs. (6)–(8). The constitutive law is applied on each microplane producing the strains on each of the 28 or 21 microplanes. The macroscopic strain is then determined numerically via integration of Eq. (9). The numerical procedure is incremental and small increments in stress are taken at each step.

4. Microplane model for cellular materials

A systematic discussion of several existing models for cellular materials in the elastic range can be found, e.g., in Grenestedt (1999). Models based on assumed microscopic mechanisms of deformation and cell morphology are given, among others, by Patel and Finnie (1969), Gibson and Ashby (1982), Christensen (1986), Warren and Kraynik (1988) and Gibson (1989). A comprehensive discussion can be found in Gibson and Ashby (1997). Many of these models seek to find a relationship between elastic moduli of the cellular material and the relative density of the material ρ/ρ_M (where ρ_M is the density of the unfoamed material), once the moduli of the unfoamed material are given. Usually such relationships are expressed in the form $E/E_M = f(\rho/\rho_M)$, where E and E_M are Young's moduli of the foam and of the unfoamed material. Analogous laws have also been derived in several ways for parameters such as yield stress, tensile strength, etc.

Here we are interested in developing a model for a closed-cell rigid foam. Phenomena such as creep (Huang and Gibson, 1990), fatigue (Harte et al., 1999) and tension–compression asymmetry (Ford and Gibson, 1998) will here be neglected. The pressure of the gas contained in the cells is neglected as well. Modeling of such aspects of the behavior of foams are left to future work.
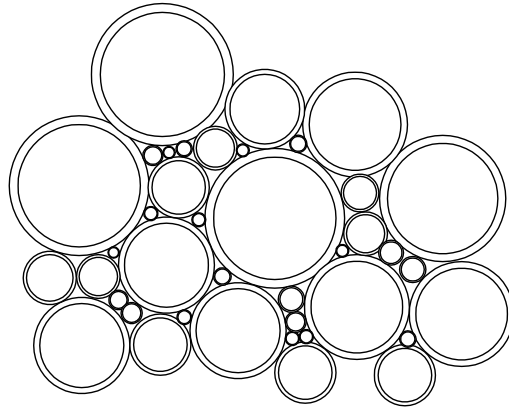
Fig. 4. Idealization of microstructure of cellular materials as a conglomerate of spheres.

We will consider the microstructure of the material to consist of hollow spherical shells which all have the same ratio of wall thickness to diameter, but different sizes (Fig. 4). Such an idealization of the microstructure was introduced, although for a different kind of analysis, by Hashin (1962).

Note the similarity between this assumed microstructure and the cell morphology shown in Fig. 1. It is assumed that many spheres of smaller sizes are distributed so that they virtually fill all the voids between larger spheres. If the ratio of thickness to radius is fixed and small, the relative density is asymptotically approximated as

$$\frac{\rho}{\rho_M} = 3\alpha, \quad \alpha = \frac{t}{R}, \tag{11}$$

where t is the thickness of a sphere and R is its radius. For a cellular material, given the relative density, α is uniquely determined by Eq. (11).

We assume that there is perfect friction, and thus no slip, between the spheres. The overall deformation of the material under a given stress state consists of the contributions of all the spheres to the deformation. We will compute such a deformation in the following approximate way.

We decompose the deformation of each sphere into a volumetric part and a part induced by deviatoric components of stress. The former part corresponds to the deformation of a hollow spherical shell under hydrostatic pressure. For the latter part, we will consider the deformation of a hollow shell under concentrated loads applied normally to its surface and corresponding to the interactions with the neighboring spheres (Fig. 5). Due to these assumptions on the mechanisms of deformation, a statically constrained microplane model appears more convenient than a kinematically constrained microplane model, for which it would be necessary to enforce the condition of zero slip between two neighboring spheres, which would be difficult.

The volumetric response for this case has been determined by Hashin (1962) (who introduced a similar microstructure to estimate the elastic moduli of heterogeneous composites):

$$\sigma_V = 3K^*\varepsilon_V, \tag{12}$$

$$K^* = \frac{4G_M K_M(\rho/\rho_M)}{4G_M + 3K_M(1 - \rho/\rho_M)} \xrightarrow[\rho/\rho_M \to 0]{} \frac{\rho}{\rho_M}\frac{4G_M K_M}{4G_M + 3K_M} = \frac{\rho}{\rho_M}\frac{2E_M}{9(1-v)}. \tag{13}$$

The deviatoric part of the deformation is computed with the microplane model by considering the microplanes as tangential to a sphere representative of the microstructure of the cellular material. On each
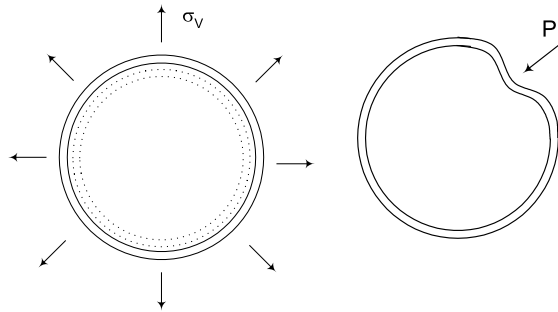
Fig. 5. Volumetric deformation of the representative sphere and deformation induced by the deviatoric components of stress.

microplane, the resolved component of deviatoric stress is considered to be acting on the surface of a spherical shell. The corresponding deformation in the elastic regime is the deformation given by Reissner (1946a,b) for a spherical cap under a concentrated load, which may be computed as the stress times the stiffness corresponding to the spherical shell. We thus have:

$$\varepsilon_D \cong \frac{u}{R} = \frac{1}{R} \frac{\sqrt{3(1-v^2)}}{4} \frac{PR}{E_M t^2} = \frac{\sqrt{3(1-v^2)}}{4} \frac{\sigma_D(4\pi R^2)/(2N)}{E_M t^2} = \frac{\sqrt{3(1-v^2)}}{E_M} \frac{\sigma_D \pi \alpha^2}{2N},$$ (14)

where u is the elastic displacement under a point load and N is the number of microplanes used for numerical integration. The foregoing expressions can be considered to be a reasonable approximation in the case of low density foams, i.e. when the relative density ρ/ρ_M is small (not more than 0.2).

As discussed in Section 2, after an initial elastic response, cellular materials usually exhibit a yield plateau, which can be the macroscopic manifestation of several microscopic phenomena: elastic buckling of cell walls (in the case of highly flexible foams), plastic yield or crushing of the walls, etc. Some of these phenomena are reversible (e.g., purely elastic buckling of cell walls in flexible foams), others are irreversible (plastic yield or crushing). Since our main interest is to model rigid foams, we simply adopt the assumption that after a certain level of stress, determined experimentally, the material response is given by Eqs. (12)–(14), where the elastic modulus of the unfoamed material is replaced by a tangential plastic modulus.

Densification can easily be reproduced through the condition that the material response be that of the bulk material if the magnitude of the compressive volumetric strain exceeds a certain value.

An important check on the validity of the model is a comparison to the experimental results and to other accepted models for the dependence of the elastic moduli of closed-cell cellular materials on their relative density; see Fig. 6 where the data are taken from Gibson and Ashby (1982). The data points in this figure are the experimental results for diverse foams and the solid line is the plot of Young's elastic modulus obtained with the present microplane model for relative densities $\rho/\rho_M < 0.2$. As it can be seen from the figure, the model is capable of capturing realistically the general trend observed experimentally for a multitude of cellular materials. Note that the line in Fig. 6 representing the predictions of the microplane model is straight. Since the scales are logarithmic, it follows that the predicted dependence of Young's modulus on the relative density is a power law. This feature agrees with other previously developed models.

Obviously a model able to accurately estimate the moduli for all cellular materials is hard to obtain, because of a number of factors that vary significantly for different materials, such as the cell geometry, the distribution of material between walls and cell edges, the amount of ''unused'' material, the variation of mechanical properties of the material constituting the matrix with the foaming process, and so on. Variations in these parameters explain the large scatter in the figure.
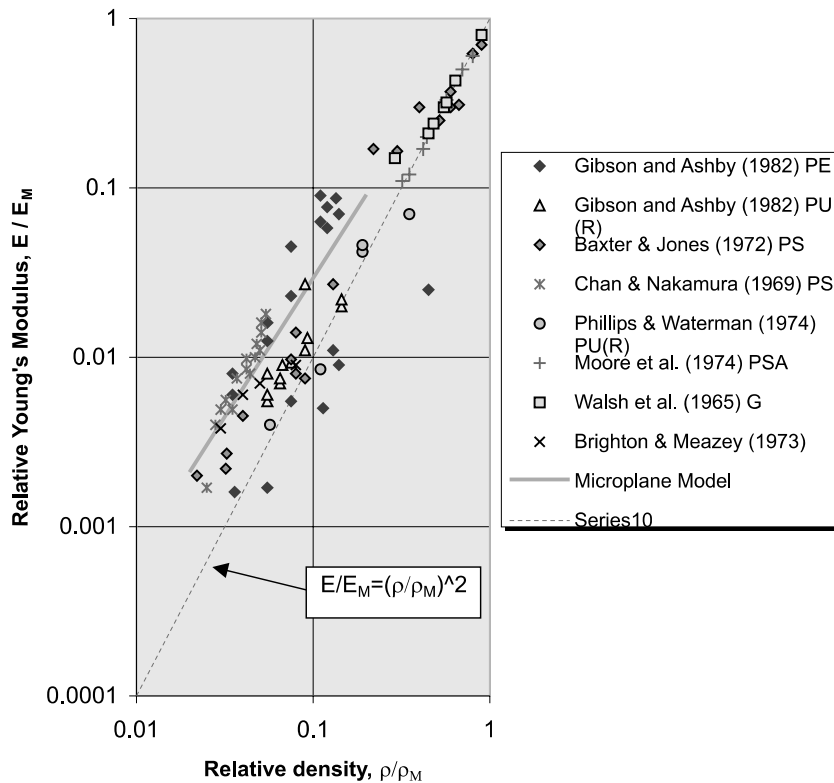
Fig. 6. Variation of elastic modulus with density of the closed-cell foam, compared to experimental data of various investigators reported by Gibson and Ashby (1982).

To employ the model for a finite element analysis such as that in Sections 6 and 7, it will be necessary for the model to exactly reproduce Young's modulus of the specific foam in the specimen or structure to be analyzed. This can be done by appropriately choosing the value for the Young's modulus of the unfoamed material that is input into the model. This value could be interpreted as the 'effective' or 'apparent' Young's modulus of the unfoamed material, and its calibration empirically takes into account all the aforementioned factors.

4.1. Zero Poisson's ratio during plastic yielding

Another important check on the model is given by the experimental results indicating that there is very little transverse deformation when a cellular material loaded uniaxially is yielding or deforming uniaxially (Shaw and Sata, 1996; Patel and Finnie, 1969; Gibson and Ashby, 1982; Neilsen et al., 1987; Neilsen, 1993). This phenomenon makes foams, unlike other materials, capable of large deformation without significant hardening even under confined conditions. This is important for technological applications where shock absorption and energy dissipation are required. Fig. 7 shows the axial and transverse strains during uniaxial loading reaching into the plastic region, as computed by the present microplane model. It can be clearly seen that the model indeed exhibits an almost zero value of "plastic Poisson's ratio"; when the yield stress is reached, the axial strain increases rapidly, while the transverse strain shows only a minor deviation from linearity.
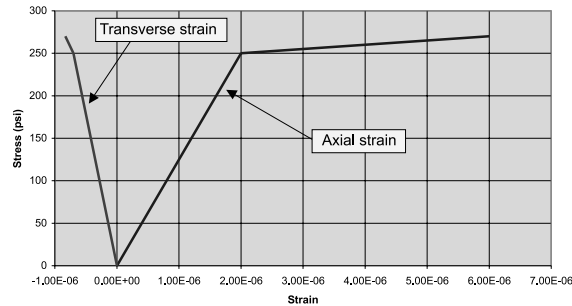
Fig. 7. Axial and transverse strain in uniaxial compression test beyond the yield point, predicted by the microplane model (the compressive strain and stress are plotted as positive).

4.2. Finite strain generalization

The model presented in this section is used in computations involving large finite strains (Ogden 1982, 1984). A discussion is therefore necessary about the proper choice of the finite strain tensor and the corresponding stress tensor. As discussed elsewhere (Bažant et al., 2000a), the modeling of various physical phenomena characterized by distinct orientations in the microstructure, such as frictional slip or microcrack growth, calls, in the case of a kinematically constrained microplane model for materials of normal (low) volume compressibility (Bažant, 1996, 1998), for the adoption of the back-rotated Cauchy stress and the Green Lagrangian strain. This stress and strain is a nonconjugate pair, acceptable only under very precise conditions verified for a broad class of materials including concrete, rock and metals, and only if certain measures making negative energy dissipation impossible are taken. As already mentioned, however, implementation of the present microplane model is more straightforward with a statically, rather than kinematically, constrained microplane model. This poses some problems, because the possibility of using a nonconjugate pair in the case of a statically constrained microplane model is questionable.

A crucial condition for the admissibility of a nonconjugate pair is that the kinematic constraint ensures the conjugacy of micro–macro constraints not just for one choice of the finite strain measure but for all the possible choices. This is one condition required for preventing negative energy dissipation. Such a condition cannot be guaranteed with the static constraint and, in this case, strict avoidance of spurious energy dissipation is therefore problematic. Facing this situation, two possible ways can be followed – implementing the present constitutive law either in (a) a kinematically constrained microplane model, by changing accordingly the microplane stress–strain relationships, or (b) in a statically constrained microplane model, with a cautious reconsideration of the choice of the stress and strain tensors to adopt. In the following, the latter alternative will be considered, which will be employed in the numerical calculations whose results are presented in Section 8.

For both the kinematically constrained and the statically constrained approaches, the stress tensor to be used is the back-rotated Cauchy stress (Bažant et al., 2000a), given by $\mathbf{s} = \mathbf{R}^\mathrm{T}\sigma\mathbf{R}$, where σ is the Cauchy stress and $\mathbf{R}$ is the material rotation tensor. This choice is dictated by the need of having a clear physical meaning for the microplane components of stress. In order for the microplane approach to retain its conceptual simplicity and retain its physical meaning, the stress components on a microplane of a certain orientation must suffice to characterize the true stresses on planes of that orientation within the material (Bažant et al., 2000a). This is valid only for the Cauchy stress.

If a statically constrained formulation is used, it is necessary to choose a conjugated pair. It can be shown that the measure of strain rate conjugated to the back rotated Cauchy stress is the back rotated deformation rate. Therefore, at each step, the increment of the strain tensor will be given by

$$\Delta\varepsilon = \mathbf{R}^{\mathrm{T}}\mathbf{D}\mathbf{R} \cdot \Delta t, \tag{15}$$

where $\mathbf{R}$ is the material rotation tensor and $\mathbf{D}$ is the rate of deformation ($\mathbf{D} = 1/2(\mathbf{L} + \mathbf{L}^{\mathrm{T}})$; $\mathbf{L} = \partial\mathbf{v}/\partial\mathbf{x} = $ velocity gradient tensor). For strain increments, the volumetric deviatoric split can be performed additively, using

$$\begin{aligned}
\Delta\varepsilon_{\mathrm{V}} &= \mathrm{tr}(\mathbf{D}), \\
\Delta\varepsilon_{ij\mathrm{D}} &= \Delta\varepsilon_{ij} - \tfrac{1}{3}\Delta\varepsilon_{\mathrm{V}}\delta_{ij},
\end{aligned} \tag{16}$$

where $\mathrm{tr}(\mathbf{D}) = \dot{J}/J$ is the rate of logarithmic volumetric strain.

The total strain, computed as $\varepsilon_{ij} = \sum \Delta\varepsilon_{ij}$, is path dependent (nonholonomic), and so it is not possible to have a unique measure of total strain, which would be needed to capture hardening or damage. This would be unsuitable for modeling materials such as concrete, for which keeping track of the total deformation with respect to the initial state is crucial. But in the case of the simple model for foams considered here, it is probably acceptable to express the constitutive law only in terms of incremental strain, without reference to the initial state. All the conditions for the inelastic response of the material are expressed in terms of total stress. For this specific case, adopting the back rotated rate of deformation as an incremental measure of strain rate is, therefore, acceptable, although this might pose some limitations to further refinements of the model. However, if strain softening had to be taken into account, then a kinematically constrained approach would offer a more solid basis.

At each step, $\Delta\varepsilon_{\mathrm{D}}$, $\Delta\varepsilon_{\mathrm{V}}$ are computed and passed to the microplane subroutine. When a statically constrained microplane model is used, trial elastic stress increments are first computed at each step of the explicit finite element computation, and then an iteration (with a Newton-Raphson algorithm) is performed until convergence on the given strain increments is reached.

4.3. Possible refinements of the model

The simple model introduced in this section is sufficient for the analysis of sandwich beams presented in the next sections. It is, however, possible to easily introduce several refinements in order to render the model capable of capturing other aspects of the mechanical behavior of foams. Here we will just briefly mention some possible modifications and additions. Further study on these issues is left to future work.

As discussed in Section 2, the response of cellular materials is usually anisotropic. During the foaming process viscous forces cause the cells to be elongated in the rise direction, and the material response will be therefore stiffer in this direction. This aspect could be introduced in the model by making Eq. (13) dependent on the orientation of the normal characterizing each microplane. As proposed by Bažant (1999), this can be done for instance by assuming that the stiffness of the material be proportional to the distance r of a point on the surface of an ellipsoid from the center of the ellipsoid (Fig. 8).

The equation of an ellipsoid centered at the origin of the coordinate system is

$$\frac{x^2}{a^2} + \frac{y^2}{b^2} + \frac{z^2}{c^2} = 1, \tag{17}$$

where $2a$, $2b$, $2c$ are the lengths of the principal axes. Setting $x = rn_1$, $y = rn_2$, $z = rn_3$, where $n_1 = \sin\theta\cos\phi$, $n_2 = \sin\theta\sin\phi$, $n_3 = \cos\theta$, one finds that

$$r = \left\{\left(\frac{n_1}{a}\right)^2 + \left(\frac{n_2}{b}\right)^2 + \left(\frac{n_3}{c}\right)^2\right\}^{-1/2}, \tag{18}$$

(n_1, n_2, n_3) is the unit vector of $\vec{r}$, normal to the microplane. Note that for $\theta = 0$, $r = c$, for $\varphi = 0$, $\theta = 90°$, $r = a$, and for $\varphi = 90°$, $\theta = 90°$, $r = b$. By choosing $a = E_x$, $b = E_y$, $c = E_z$, one obtains Bažant's (1999)
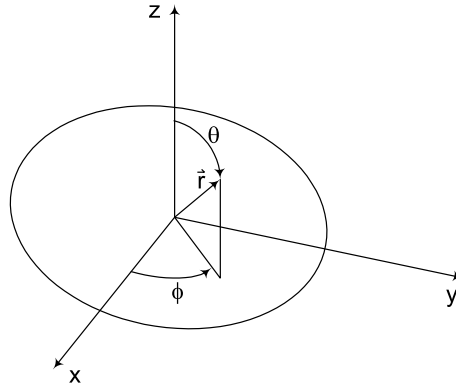
Fig. 8. An ellipsoid, with vector $\vec{r}$ defining a generic point on the surface.

expression for the elastic modulus associated with a microplane normal to vector $\vec{r}$, characterized by θ and ϕ:

$$E_{\mathrm{N}} = E_{\vec{r}} = \left\{ \left(\frac{n_1}{E_x} \right)^2 + \left(\frac{n_2}{E_y} \right)^2 + \left(\frac{n_3}{E_z} \right)^2 \right\}^{-1/2}. \tag{19}$$

A microplane model for cellular material with such a dependence of the microplane Young's modulus on the orientation of the microplanes has been implemented and used to determine the variation of the overall modulus of the material with the direction. The results of this study are shown in Fig. 9. Usually cellular materials exhibit transverse isotropy and therefore $E_x = E_y < E_z$, z being the rise direction. The first curve in Fig. 9 gives the variation of the uniaxial modulus with the direction, when the direction is varied in the xz plane. The second curve gives the variation in the xy plane. Obviously in this second case the modulus is constant.

The simple model introduced in this section is meant to reproduce the behavior of rigid foams, for which the elastic deformation is small. The cell walls of flexible foams can undergo large recoverable elastic strains. Thus, in the case of flexible foams, the model would have to be refined in order to take into account the possibility of large deformations in Eqs. (12) and (14). Doing so would imply considering the possibility of elastic buckling of the cell walls, and in this case the interaction among microplanes would be very significant. A study of this aspect is left to future work.
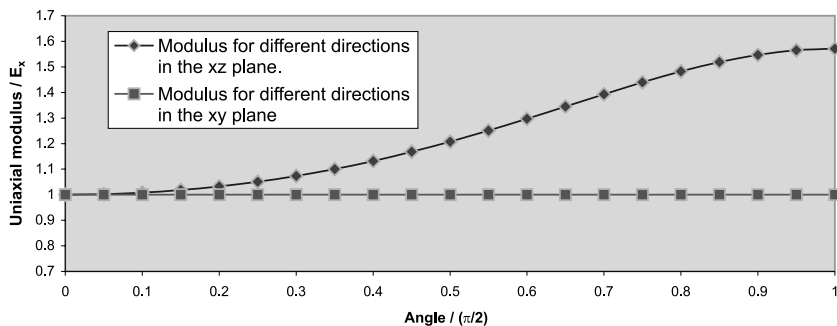

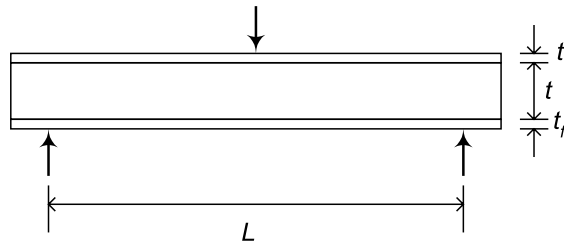Fig. 9. Variation of the uniaxial modulus with the direction as computed with the microplane model.

Fig. 10. Dimensions of the specimens for the three-point bending tests.

The last possible refinement to be mentioned here regards the asymmetric behavior of cellular materials in tension and compression (see Section 2). It could be modeled by a modification of the microplane constitutive laws. Tension–compression asymmetry is however neglected here and its study is left for future work.

5. Experimental studies on sandwich beams

Sandwich beams can fail in several different ways. A systematic discussion of failure modes for sandwich beams with foam cores can be found, e.g., in Triantafillou and Gibson (1987) and Daniel et al. (2000). Since the main interest in this study is in the modeling of foam, we will consider, among the possible failure modes, that which is governed by finite strain deformation of the foam core, that is, the failure by core indentation.

Some tests exhibiting failure by core indentation have been performed by Daniel et al. (1999, 2000) and Daniel and Abot (2000). Here three-point bending tests on two specimens will be considered (Fig. 10). The specimens of type (a) have core thickness $t = 25$ mm (0.984 in.), and the specimens of type (b) have core thickness $t = 50$ mm (1.968 in.). The other dimensions are common to both kinds of specimens: span $L = 360$ mm (14.17 in.), facing thickness $t_f = 1$ mm (0.04 in.).

The material used for the core is a rigid polyvinyl chloride (PVC) foam (Divinycell H100 foam). PVC is a thermoplastic amorphous polymer also used to produce flexible, open-cell, and low to medium density foams. Rigid PVC foams have low flammability. They have an almost completely closed-cell structure and therefore low water absorption.

The material used for the facings is AS-4/3501-6 carbon-epoxy composite. In these tests, the final failure is caused by breaking of the carbon-epoxy facings. However, before failure the core deforms largely in proximity of the point of application of the load and foam deformation affects significantly the overall mechanical response up to failure.

6. Finite element analysis of failure of sandwich beams by core indentation

Finite element analysis of the tests is performed with a three-dimensional explicit finite element code implemented with an updated Lagrangian formulation. Dynamic relaxation is used to reproduce the quasi-static nature of the loading process. The domain is discretized by standard eight-node brick elements. The foam core is modeled with the microplane model presented in Sections 3 and 4. A three-dimensional code is used for the analysis because the stress condition for the foam varies from approximately plane strain condition close to the facings, where the lateral expansion is prevented by the relatively high stiffness of the carbon-epoxy composite, to approximately plane stress close to the midplane of the beam.
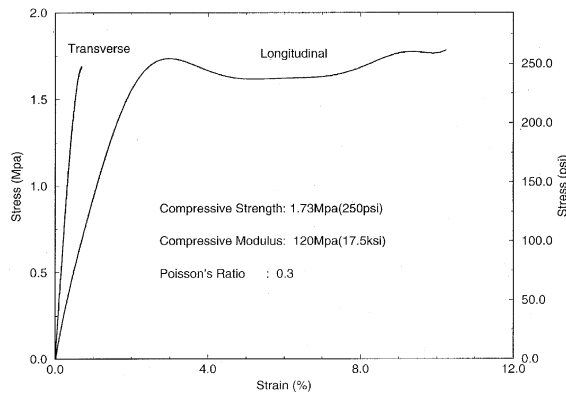
Fig. 11. Measured stress–strain curves for Divinicell H100 under uniaxial compression.

6.1. Polyvinyl chloride foam

The microplane model for a closed-cell cellular material introduced in Section 4 is used to model the Divinicell H100 foam. The stress value at which the response ceases to be elastic is determined from a uniaxial test (Fig. 11). Since, in the uniaxial test, the material exhibits a substantially flat yield plateau, a number close to zero is adopted for the tangential plastic modulus.

As already mentioned, tension–compression asymmetry is neglected at this point and only the data for the compressive behavior of the PVC foam are used to set the material parameters in the model. This simplification seems to be acceptable for the analysis of three-point bending of sandwich beams, during which nonlinear behavior of the core is expected mainly in the regions subjected to compression.

7. Modeling of the facings

The properties of the AS-4/3501-6 carbon-epoxy composite used for the facings are shown in Table 1. The thickness of the facings is 1 mm (0.04 in.) for both cases considered here.

Table 1
Mechanical properties of unidirectional AS4/3501-6 carbon/epoxy

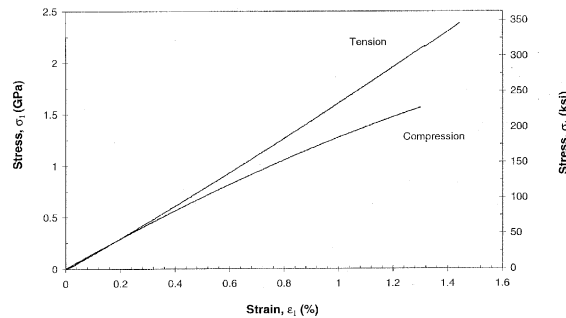| Property	Value
Fiber volume ratio, V_f	0.70
Longitudinal elastic modulus, E_1, GPa (Msi)	146.6 (21.26)
Transverse elastic modulus, E_2, GPa (Msi)	72.4 (10.5)
In-plane shear modulus, G_{12}, GPa (Msi)	7.6 (1.1)
Major Poisson's ratio, v_{12}	0.28
Minor Poisson's ratio, v_{21}	0.02
Longitudinal tensile strength, F_{1t}, MPa (ksi)	2386 (346)
Longitudinal compressive strength, F_{1c}, MPa (ksi)	1627 (235)
In-plane shear strength, F_{12}, MPa (ksi)	71 (10.3)
Ultimate tensile strain, ε_{1t}^u, (%)	1.45
Ultimate compressive strain, ε_{1c}^u, (%)	1.36
Ultimate in-plane shear strain, ε_{12}^u, (%)	0.75
Transverse tensile strength, F_{2t}, MPa (ksi)	64 (9.3)
Transverse compressive strength, F_{2c}, MPa (ksi)	228 (33)

Fig. 12. Longitudinal tensile and compressive stress–strain behavior of AS-4/3501-6 unidirectional carbon-epoxy composite.
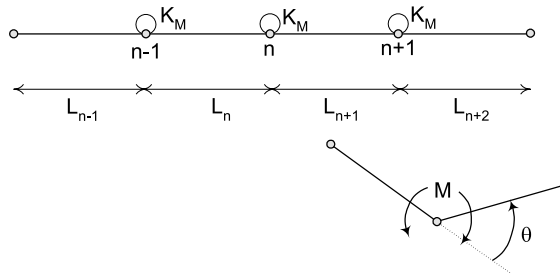

Fig. 13. Truss elements with flexural springs.

The inelastic behavior of this material is slightly asymmetric in tension and compression (Fig. 12). However, the maximum average tensile and compressive stress in the facings can be estimated as about 60 ksi for specimen (b) at peak load. Such a value of stress is within a range in which it is reasonable to assume that the material behavior is linearly elastic. Therefore, the axial stress transmitted along the truss elements has been computed as the stress for a linear elastic material.

For convenience of programming, the two carbon-epoxy sheets, placed at the top and bottom of the sandwich beam, have been modeled not as beam elements but as inflexible bar elements connected by flexural springs at the nodes (Fig. 13). The computation of the bending moment transmitted by the flexural springs at the nodes is somewhat complicated due to the fact that the curvature of the sheet under the point of application of the load is such that the material undergoes stresses and strains reaching into the inelastic region. We will thus first introduce the concept of flexural springs for a linear elastic material and then we will discuss its extension to the case of a nonlinear material.

The flexural springs transmit a bending moment, M, which depends on the relative rotation of two neighboring truss elements. For a linear elastic material, $M = K_{\mathrm{M}}\theta$.

To compute the value of K_{M} at a given node n, we compute θ, defined as shown in Fig. 13, and assume that there is a uniform curvature along the two adjacent elements, $\kappa = \theta/[(L_n + L_{n+1})/2]$. The bending moment at node n will therefore be $M = \kappa \cdot EI = \theta EI/[(L_n + L_{n+1})/2]$, from which we have $K_{\mathrm{M}} = EI/[(L_n + L_{n+1})/2]$, where E is the Young's modulus of carbon composite and I is the moment of inertia of the cross-section of the sheet relevant for node n. For this computation we consider flexural stiffness only for curvature in the plane of the axis of the beam.

For a nonlinear material, K_{M} is not constant, but depends on the current θ and in general on the history of θ. For the sake of simplicity, we will assume here only a dependence on the current θ, which is valid in the case of a loading history with monotonically increasing θ, as expected in the case of the three point bending test considered here.
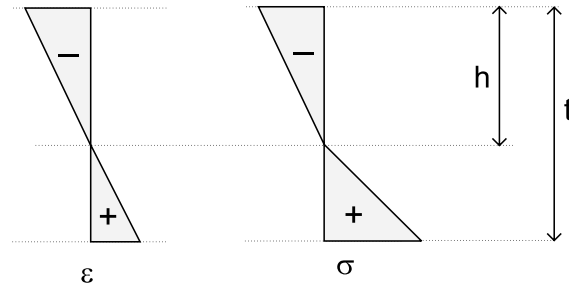
Fig. 14. Assumed strain and stress distribution along the thickness of nonlinear facings.

From the experimental curves shown in Fig. 12, we observe that the tangential elastic modulus in tension just before failure is $E_T^M \cong 1.25E$ (where E is the initial Young's modulus of the material), and the tangential elastic modulus in compression just before failure is $E_C^m \cong 1/2E_T^M$. As a first approximation we consider the flexural stiffness of the sheet at failure by assuming that the material response in compression is characterized by E_C^m, whose value is constant within the portion of the cross-section under compression, and the material response in tension is characterized by $E_T^M = 2E_C^m$. For such a simplified case, the position of the neutral axis is easily calculated as given by $h = 0.585t$, where h and t are defined according to Fig. 14.

Compared to the linear flexural stiffness, the corresponding flexural stiffness is reduced and is approximately given by $K_M^f = 0.85K_M^{el}$. For the sake of simplicity, it is assumed that the flexural stiffness varies linearly with the curvature, from the initial value K_M, to the final value K_M^f, at which the curvature κ reaches the ultimate admissible value κ_u:

$$K_M = K_M^{el} - \frac{\kappa}{\kappa_u}(1 - K_M^u). \tag{20}$$

The value of κ_u is estimated, under the assumption of stress and strain distributions shown in Fig. 14, as the value of κ for which the compressive strain reaches the ultimate compressive strain value κ_u. For the material considered here, $\kappa_u \cong 0.6$ rad/in.

In the three-point bending tests considered here, failure always occurs by breaking of the carbon-epoxy facings. A failure criterion for the facings must therefore be introduced in the analysis in order to capture the maximum deflection sustained by the beams. It is considered that failure occurs if κ at any node of the facings exceeds κ_u.

8. Numerical results

Two specimen sizes have been considered: specimen (a) has core thickness $t_c = 25$ mm (0.984 in.), specimen (b) has core thickness $t_c = 50$ mm (1.968 in.).

Fig. 15a shows the mesh used for the analysis of specimen (a), with the truss elements used for the facings. Fig. 15b shows the deformed mesh at the end of the computation of specimen (a). Indentation can be clearly seen at the center of the specimen under the load. Fig. 16 shows the load–displacement curve obtained numerically and the experimental ones. Figs. 17a,b and 18 show the results of the analysis of specimen (b).

Failure in the thicker beams (specimen (b)) occurs after a smaller deflection, because the indentation of the core is such as to cause breaking of the facings at an earlier stage than for the case of specimen (a). This is captured correctly by the finite element analysis.
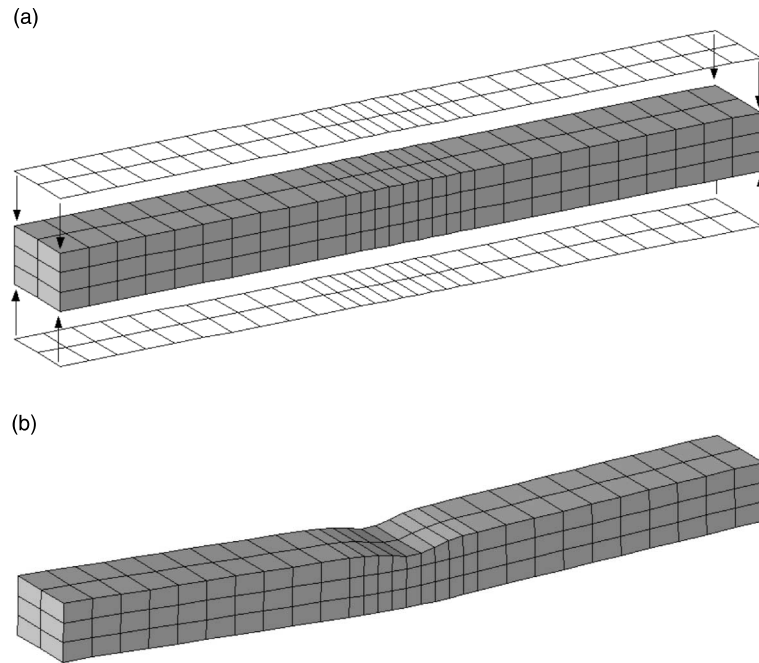
(a)

(b)

Fig. 15. (a) Mesh for the analysis of specimen (a). (b) Deformed mesh at the end of the loading process (specimen (a)).
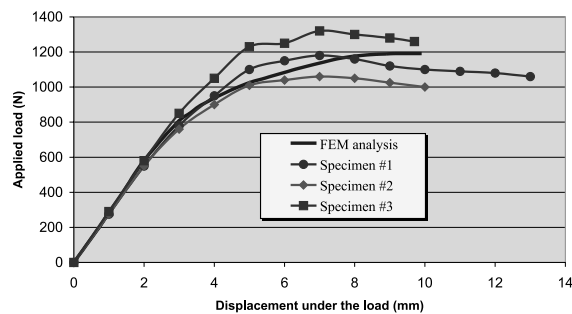

Fig. 16. Load–displacement diagrams (experimental and computed) for specimen type (a).

Note that there is no lateral bulging of the foam in the region under the point of application of the load. This confirms that the model exhibits "zero plastic Poisson ratio".

9. Softening behavior and size effect

Even when the material used for the core does not exhibit softening (as is the case for the PVC foam used for the sandwich beams considered in this paper), the sandwich beam as a whole can nevertheless exhibit structural softening in the load–deflection diagram. This is due to a reduction of the cross-sectional area of beam and a decrease of separation of the faces, and hence of the bending stiffness, caused by large deformations in the core.
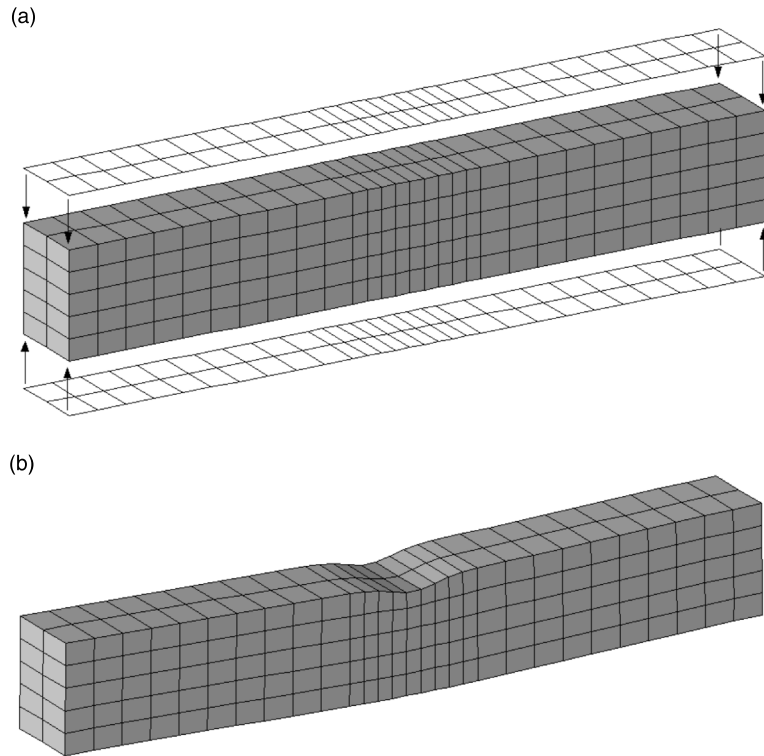
(a)

(b)

Fig. 17. (a) Mesh for the analysis of specimen (b). (b) Deformed mesh at the end of the loading process (specimen (b)).
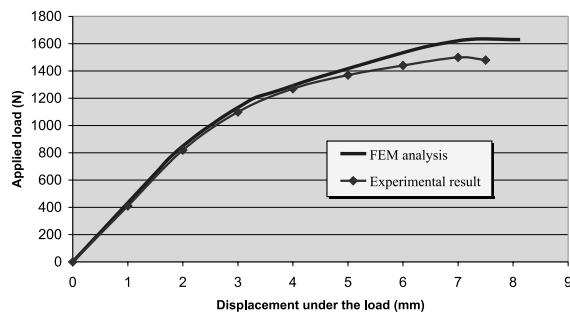
Fig. 18. Load–displacement diagrams (experimental and computed) for specimen type (b).

Considering geometrically similar beams of different sizes, one must expect the localized reduction of flexural stiffness in the beam to be the source of a size effect (Bažant et al., 1987), that is, a reduction of the nominal strength of beam with increasing size (the nominal strength being defined as the maximum load divided by the cross-sectional area). This aspect of the structural behavior of sandwich beams is currently under study.

10. Conclusions

A new microplane model for closed-cell stiff foams has been formulated. The model is shown to be able to reproduce the major features of the mechanical behavior observed experimentally.

In particular, the correct experimentally observed dependence of Young's modulus on mass density is obtained. A zero plastic Poisson's ratio is naturally exhibited by the model. A simple approach for dealing with anisotropy is formulated and investigated. Various possible extensions or modifications are pointed out and discussed.

The results of finite element analysis of three-point bending tests of sandwich beams, carried out with the new model, show that the model can be successfully used for structural analysis. Core indentation, leading to failure of sandwich beam and involving large deformations of the foam core, is realistically reproduced by the analysis, in agreement with previous experiments.

References

Batdorf, S.B., Budiansky, B., 1949. A mathematical theory of slip based on the concept of slip. National Advisory Committee for Aeronautics TN, 1871.

Bažant, Z.P., 1984. Microplane model for strain controlled inelastic behavior. In: Desai, C.S., Gallagher, R.H. (Eds.), Mechanics of Engineering Materials, Wiley, London, pp. 45–59 (Chapter 3).

Bažant, Z.P., 1996. Finite strain generalization of small strain constitutive relations for any finite strain tensor and additive volumetric–deviatoric split. International Journal of Solids and Structures 33 (20–22), 2887–2897 (special issue in memory of Juan Simo).

Bažant, Z.P., 1998. Easy to compute finite strain tensors with symmetric inverse, approximating Hencky strain tensor. ASME Journal of Materials and Technology, 120 (April), 131–136.

Bažant, Z.P., 1999, private communication.

Bažant, Z.P., Adley, M.D., Carol, I., Jirasek, M., Akers, S.A., Rohani, B., Cargile, J.D., Caner, F.C., 2000a. Large-strain generalization of microplane model for concrete and applications. ASCE Journal of Engineering Mechanics, 126 (9), 971–980.

Bažant, Z.P., Caner, F.C., Adley, M.D., Akers, S.A., 2000b. Incorporation of rate effects of fracturing and creep into microplane model M4 for concrete dynamics. ASCE Journal of Engineering Mechanics, 126 (9), 962–970.

Bažant, Z.P., Caner, F.C., Carol, I., Adley, M.D., Akers, S.A., 2000c. Microplane model M4 for concrete: I. Formulation with work-conjugate deviatoric stress. ASCE Journal of Engineering Mechanics, 126 (9), 944–953.

Bažant, Z.P., Pan, J.-Y., Pijaudier-Cabot, G., 1987. Softening in reinforced concrete beams and frames. ASCE Journal of Structural Engineering 113 (12), 2333–2347.

Bažant, Z.P., Prat, P., 1987. Creep of anisotropic clay: new microplane model. ASCE Journal of Engineering Mechanics 103 (7), 1050–1064.

Bažant, Z.P., Prat, P.C., 1988a. Microplane model for brittle plastic materials: I. Theory. ASCE Journal of Engineering Mechanics 114 (10), 1672–1688.

Bažant, Z.P., Prat, P.C., 1988b. Microplane model for brittle plastic materials: II. Verification. ASCE Journal of Engineering Mechanics 114 (10), 1689–1702.

Bažant, Z.P., Oh, B.H., 1985. Microplane model for progressive fracture of concrete and rock. ASCE Journal of Engineering Mechanics 111, 559–582.

Bažant, Z.P., Oh, B.H., 1986. Efficient numerical integration on the surface of a sphere. Zeitschrift für angewandte Mathematik und Mechanik (ZAMM, Berlin) 66 (1), 37–49.

Bažant, Z.P., Xiang, Y., Prat, P.C., 1996. Microplane model for concrete. I. Stress–strain boundaries and finite strain. ASCE Journal of Engineering Mechanics 122 (3), 245–254, Errata, vol. 123, 411.

Brocca, M., Bažant, Z.P., 2000. Microplane constitutive model and metal plasticity. Applied Mechanics Reviews, ASME 53 (10), 265–281.

Brocca, M., Brinson, C., Bažant, Z.P., 2000. Microplane constitutive model for shape memory alloys. Report, Northwestern University.

Budiansky, B., Wu, T.T., 1962. Theoretical prediction of plastic strains in polycrystals. Proceedings of the Fourth US National Congress of Applied Mechanics, 1175–1185.

Carol, I., Bažant, Z.P., 1997. Damage and plasticity in microplane theory. International Journal of Solids and Structures 34 (29), 3807–3835.

Chang, F.S., Song, Y., Lu, D.X., 1998. Unified constitutive equations of foam materials. Journal of Engineering Materials and Technology 120, 212–217.

Christensen, R.M., 1986. Mechanics of low density materials. Journal of the Mechanics of Physics and Solids 34, 563–578.

Daniel, I.M., Abot, J.L., Wang, K.A., 1999. Testing and analysis of composite sandwich beams. ICCM12, Twelfth International Conference on Composite Materials, Paris.

Daniel, I.M., Gdoutos, E.E., Wang, K.A., Abot, J.L., 2000. Failure modes of composite sandwich beams, ICTAM 2000 Conference, Chicago, International Journal of Damage Mechanics, submitted for publication.

Daniel, I.M., Abot, J.L., 2000. Fabrication, testing and analysis of composite sandwich beams. Composites Science and Technology 60 (12–13), 2455–2463.

Ford, C.M., Gibson, L.J., 1998. Uniaxial strength asymmetry in cellular materials: an analytical model. International Journal of Mechanical Sciences 40 (6), 521–531.

Gibson, L.J., 1989. Modeling the mechanical behavior of cellular materials. Materials Science and Engineering A 110, 1–36.

Gibson, L.J., Ashby, M.F., 1982. The mechanics of three-dimensional cellular solids. Proceedings of the Royal Society of London 382, 43.

Gibson, L.J., Ashby, M.F., 1997. Cellular Solids: Structure and Properties, Pergamon Press, Oxford.

Grenestedt, L.J., 1999. Effective elastic behavior of some models for 'perfect' cellular solids. International Journal of Solids and Structures 36, 1471–1501.

Harte, A.-M., Fleck, N.A., Ashby, M.F., 1999. Fatigue failure of an open cell and a closed cell aluminum alloy foam. Acta Materialia 47 (8), 2511–2524.

Hashin, Z., 1962. The elastic moduli of heterogeneous materials. Journal of Applied Mechanics 29, 143–150.

Hill, R., 1965. Continuum micromechanics of elastoplastic polycrystals. Journal of the Mechanics and Physics of Solids 13, 89–102.

Hill, R., 1966. Generalized constitutive relations for incremental deformation of metal crystals by multislip. Journal of the Mechanics of Physics and Solids 14, 95–102.

Huang, J.-S., Gibson, L.J., 1990. Creep of sandwich beams with polymer foam cores. Journal of Materials in Civil Engineering 2 (3), 171–182.

Huber, A.T., Gibson, L.J., 1988. Anisotropy of foams. Journal of Materials Science 23, 3031–3040.

Kröner, E., 1961. Zur plastischen Verformung des Vielkristalls. Acta Metallica 9, 155–161.

Lin, T.H., Ito, M., 1965. Theoretical plastic distortion of a polycrystalline aggregate under combined and reversed stresses. Journal of the Mechanics and Physics of Solids 13, 103–115.

Neilsen, M.K., Morgan, H.S., Krieg, R.D., 1987. A Phenomelogical Constitutive Model for Low Density Polyurethane Foams. Sandia National Laboratories, Albuquerque New Mexico, SAND86-2927.

Neilsen, M.K., 1993. Continuum Representation of Cellular Solids. Sandia National Laboratories, Albuquerque New Mexico, SAND93-1287.

Ogden, R.W., 1982. Elastic deformation in rubberlike solids. In: Hopkins, H.G., Sewell, M.J. (Eds.), Mechanics of Solids, the Rodney Hill 60th Anniversary Volume, 499–537.

Ogden, R.W., 1984. Non-linear Elastic Deformations. Ellis Horwood, Wiley, Chichester, UK.

Pande, G., Sharma, K., 1983. Multilaminate model of clays – a numerical evaluation of the influence of rotation of principal axes. ASCE Journal of Engineering and Mechanics 109 (7), 397–418.

Patel, M.R., Finnie, I., 1969. The deformation and fracture of rigid cellular plastics under multiaxial stress. Lawrence Livermore National Laboratory, Livermore California, UCRL-13420.

Prat, P., Bažant, Z.P., 1989. Microplane model for triaxial deformation of soils. In: Pietruszac, S., Pande, G. (Eds.), Numerical Models in Geomechanics (NUMOG III), Elsevier, Niagara Falls, Canada, pp. 139–146.

Prat, P., Bažant, Z.P., 1991a. Microplane model for triaxial deformation of saturated cohesive soils. ASCE Journal of Geotechnical Engineering 117 (6), 891–912.

Prat, P., Bažant, Z.P., 1991b. A time dependent microplane model for creep of cohesive soils. In: Adeli, H., Sierakowski, R.L. (Eds.), Mechanics Computing in the 90s and beyond, Proceedings. of the ASCE-EMD Specialty Conference, ASCE, Columbus, Ohio, USA, pp. 1224–1228.

Puso, M.A., Govindjee, S., 1995. A phenomenological constitutive model for rigid polymeric foam. ASME Material Division Publications 68, 159–176.

Reissner, E., 1946a. Stresses and small displacements of shallow spherical shells: I. International Journal of Mathematics and Physics 25, 80–85.

Reissner, E., 1946b. Stresses and small displacements of shallow spherical shells: II. Journal of Mathematics and Physics 25, 279–300.

Rice, J.R., 1971. Inelastic constitutive relations for solids: an internal variable theory and its application to metal plasticity. Journal of the Mechanics and Physics of Solids 19, 433–455.

Shaw, M.C., Sata, T., 1966. The plastic behavior of cellular materials. International Journal of Mechanical Sciences 8, 469.

Stroud, A.H., 1971. Approximate calculation of multiple integrals. Prentice-Hall, Englewood Cliffs, NJ.

Taylor, G.I., 1938. Plastic strain in metals. Journal of the Institute of Metals 63, 307–324.

Triantafillou, T.C., Gibson, L.J., 1987. Failure mode maps for foam core sandwich beams. Materials Science and Engineering 95, 37–53.

Warren, W.E., Kraynik, A.M., 1988. The linear elastic properties of open-cell foams. Journal of Applied Mechanics 55, 341–346.

Zienkiewicz, O., Pande, G., 1977. Time-dependent multi-laminate model of rocks – a numerical study of deformation and failure of rock masses. International Journal of Analytical and Numerical Methods in Geomechanics 1, 219–247.